
EMPIRICAL OPTIMAL TRANSPORT BETWEEN CONDITIONAL DISTRIBUTIONS

A PREPRINT

Piyushi Manupriya Rachit Keerti Das Sayantan Biswas Shivam Chandhok* J. Saketha Nath

IIT Hyderabad, India

ABSTRACT

Given samples from two joint distributions, we consider the problem of Optimal Transportation (OT) between the corresponding distributions conditioned on a common variable. The objective of this work is to estimate the associated transport cost (Wasserstein distance) as well as the transport plan between the conditionals as a function of the conditioned value. Since matching conditional distributions is at the core of supervised training of discriminative models and (implicit) conditional-generative models, OT between conditionals has the potential to be employed in diverse machine learning applications. However, since the conditionals involved in OT are implicitly specified via the joint samples, it is challenging to formulate this problem, especially when (i) the variable conditioned on is continuous and (ii) the marginal of this variable in the two distributions is different. We overcome these challenges by employing a specific kernel MMD (Maximum Mean Discrepancy) based regularizer that ensures the marginals of our conditional transport plan are close to the conditionals specified via the given joint samples. Under mild conditions, we prove that our estimator for this regularized transport cost is statistically consistent and derive finite-sample bounds on the estimation error. Application-specific details for parameterizing our conditional transport plan are also presented. Furthermore, we empirically evaluate our methodology on benchmark datasets in applications like classification, prompt learning for few-shot classification, and conditional-generation in the context of predicting cell responses to cancer treatment.

1 Introduction

Optimal Transport (OT) has emerged as a powerful tool for comparing distributions and has been successfully applied in diverse machine learning applications [Peyré and Cuturi, 2019, Liu et al., 2020, Fatras et al., 2021, Cao et al., 2022, Chen et al., 2023]. However, one often needs to compare conditional distributions: for e.g., in supervised learning of (probabilistic) discriminative models, one needs to compare the model’s label posterior with that corresponding to the training data. Similar is the case with (implicit) conditional-generative models. In such applications, the observed input covariates are rarely discrete, and hence multiple samples for a given input cannot be assumed. Hence it is not clear how OT can be performed between the relevant conditionals as they are implicitly defined via samples from the input-label joint. Moreover, in medical domain applications like treatment-effect prediction [Hahn et al., 2019], the distribution of input covariates for the treated and untreated patients are different. Hence, merely performing OT between the joint distributions of input and label (treatment outcome) is not the same as comparing the corresponding conditionals.

In this paper, we address this challenging problem of performing OT between two distributions when conditioned on a common variable, say $s(y/x)$ and $t(y/x)$, using samples from the joint distributions, $s(x, y), t(x, y)$. As motivated earlier, we do not restrict the variable x to be discrete, and we do not make the assumption that the marginals of the common variable are the same, i.e., we do not assume $s(x) = t(x)$. In this setting, we present novel estimators for the corresponding optimal transport cost and transport plan as a function of x .

Few earlier works have attempted to solve this problem in some special cases. [Frogner et al., 2015] presents an estimator for the special case $s(x) = t(x)$ and y being discrete. Their estimator does not readily generalize to the case

*Work done while working at IIT-Hyderabad.

where y is continuous. Also, they do not model the transport map/plan as a function of x and rather solve individual OT problems at every x . [Tabak et al., 2021] begin with the general problem, but since they employ a KL divergence-based regularizer, their formulation simplifies to performing OT between the joint distributions (refer to equation (4) in their paper). We instead use a MMD (Maximum Mean Discrepancy) based regularizer that maintains the critical distinction between matching conditionals vs joints and also facilitates non-parametric matching with the empirical conditionals. Finally, [Bunne et al., 2022] consider special applications where multiple samples from $s(y/x), t(y/x)$ are available and learn a transport map as a function of x by solving standard OT problems between $s(y/x), t(y/x)$ individually for the given x samples. Also, their approach assumes the ground cost function to be the squared Euclidean. In contrast, we do not assume that multiple samples from $s(y/x), t(y/x)$ are available and do not restrict the ground cost to be Euclidean. Further, we also estimate the transport plan rather than the transport map. Owing to these reasons, our methodology is more widely-applicable. In summary, existing works consider special cases of our problem and present estimators for the transport map. To the best of our knowledge, we are the first to address the general problem of OT between conditionals described above leading to provably consistent estimators for the optimal transport cost as well as the transport plan as a function of x .

The key idea in our formulation is to employ an MMD-based regularizer for enforcing the marginal constraints. Since these marginal constraints themselves involve the conditionals $s(y/x)$ and $t(y/x)$, while samples from the joints, $s(x, y), t(x, y)$, are only available, we present a kernel regression type estimator for these MMD terms. We then present the overall sample-based formulation for performing OT between conditionals involving these MMD estimators. Under mild assumptions, we are able to show that our estimator for the optimal transport cost (Wasserstein distance) between $s(y/x)$ and $t(y/x)$ is statistically consistent. Using standard concentration inequalities, we also derive bounds on the estimation error with finite-samples.

Another point of deviation from the earlier works, [Bunne et al., 2022] [Tabak et al., 2021], is that we model the transport plan, $\pi(y, y'/x)$, as a function of x . Moreover, we model the plan via modelling its factors: $\pi(y'/y, x)\pi(y/x)$. This gives a two-fold advantage: (A) This factorization simplifies our formulation when dealing with discriminative/conditional-generative models by allowing us to directly choose $\pi(y/x)$ to be the same as that defined by the discriminative/conditional-generative model to be learnt. (B) When modelled implicitly, the factor $\pi(y'/y, x)$ enables one-to-many inferences (e.g., see Figure 1b in [Korotin et al., 2023]) rather than one-to-one inferences implied by a transport map.

We validate the correctness of our estimator through synthetic experiments. We present different variants of our formulations and show the utility of the proposed formulation in diverse applications.

Contributions

- To the best of our knowledge, we are the first to present a consistent estimator for optimal transport cost in the context of the general conditional optimal transport problem.
- Unlike the popular KL-based regularization [Frogner et al., 2015], [Tabak et al., 2021], we employ MMD-regularization that helps us match conditionals rather than joints even when the variables involved are continuous.
- We present a theoretical analysis of our estimator and prove its statistical consistency.
- We model the transport plan rather than the transport map [Tabak et al., 2021], [Bunne et al., 2022], which enables more general inferences.
- We empirically evaluate the proposed formulation on applications like classification, prompt learning for few-shot classification, and conditional-generation in the context of predicting cell responses to cancer treatment.

2 Background

Let \mathcal{X}, \mathcal{Y} be two sets (domains) that form compact Hausdorff spaces. Let $\mathcal{P}(\mathcal{X})$ be the set of all probability measures over \mathcal{X} .

Optimal Transport (OT) Given a cost function, $c : \mathcal{Y} \times \mathcal{Y} \mapsto \mathbb{R}$, OT compares two measures $s, t \in \mathcal{P}(\mathcal{Y})$ by finding a plan to transport mass from one to the other, that incurs the least expected cost. More formally, Kantorovich’s OT formulation is given by:

$$W_c(s, t) \equiv \min_{\pi \in \mathcal{P}(\mathcal{Y} \times \mathcal{Y})} \int c d\pi, \text{ s.t. } \pi_1 = s, \pi_2 = t, \quad (1)$$

where π_1, π_2 are the marginals of π . When the cost is a valid metric over \mathcal{Y} , then $W(s, t)$ is a valid metric between the measures $s, t \in \mathcal{P}(\mathcal{Y})$, popularly known as the Wasserstein metric.

Table 1: Summary of related works

	[Tabak et al., 2021]	[Bunne et al., 2022]	COT
OT between conditionals	×	✓	✓
Flexibility with the ground cost	✓	×	✓
Allows single sample per conditioned variable	✓	×	✓
Models OT plan	×	×	✓
Flexibility of Implicit modelling	N/A	N/A	✓

Maximum Mean Discrepancy (MMD) Given a characteristic kernel function [Sriperumbudur et al., 2011], $k : \mathcal{Y} \times \mathcal{Y} \mapsto \mathbb{R}$, MMD defines a metric over probability measures given by: $\text{MMD}^2(s, t) \equiv \mathbb{E}_{X \sim s, X' \sim s}[k(X, X')] + \mathbb{E}_{Y \sim t, Y' \sim t}[k(Y, Y')] - 2\mathbb{E}_{X \sim s, Y \sim t}[k(X, Y)]$. With \mathcal{H}_k as the RKHS associated with the characteristic kernel k , the dual norm definition of MMD is given by $\text{MMD}(s, t) = \max_{f \in \mathcal{H}_k; \|f\| \leq 1} \mathbb{E}_s[f(X)] - \mathbb{E}_t[f(Y)]$.

Total Variation (TV) Total Variation is another popular metric over probability measures defined by: $\text{TV}(s, t) \equiv \int_{\mathcal{Y}} d|s - t|(y)$, where $|s - t|(y) \equiv \begin{cases} s(y) - t(y) & \text{if } s(y) \geq t(y) \\ t(y) - s(y) & \text{otherwise} \end{cases}$.

3 Problem Formulation

This section formally defines the Conditional Optimal Transport (COT) problem and presents a consistent estimator for it in the general setting. We begin by recalling the definition of OT between two given measures $s(y/x), t(y/x)$:

$$W_c(s(y/x), t(y/x)) \equiv \min_{\pi \in \mathcal{P}(\mathcal{Y} \times \mathcal{Y})} \int_{\mathcal{Y} \times \mathcal{Y}} c \, d\pi, \text{ s.t. } \pi_1 = s(y/x), \pi_2 = t(y/x), \quad (2)$$

If the cost is a valid metric, then $W_c(s(y/x), t(y/x))$ is nothing but the Wasserstein distance between $s(y/x), t(y/x)$. In typical learning applications, one needs to compare the expected Wasserstein distance over a distribution of inputs, say $a \sim \mathcal{P}(\mathcal{X})$, rather than at a particular input. Accordingly, we consider $\mathbb{E}_{X \sim a}[W_c(s(y/X), t(y/X))]$:

$$\begin{aligned} & \int_{\mathcal{X}} \min_{\substack{\pi(x) \in \mathcal{P}(\mathcal{Y} \times \mathcal{Y}) \\ \forall x \in \mathcal{X}}} \int_{\mathcal{Y} \times \mathcal{Y}} c \, d\pi(x) da, \text{ s.t. } \pi_1(x) = s(y/x), \pi_2(x) = t(y/x) \forall x \in \mathcal{X}, \\ & \equiv \min_{\pi: \mathcal{X} \mapsto \mathcal{P}(\mathcal{Y} \times \mathcal{Y})} \int_{\mathcal{X}} \int_{\mathcal{Y} \times \mathcal{Y}} c \, d\pi(x) da, \text{ s.t. } \pi_1(x) = s(y/x), \pi_2(x) = t(y/x) \forall x \in \mathcal{X}. \end{aligned} \quad (3)$$

In the special case where the auxiliary measure, a , is degenerate (3) gives back (2). Henceforth we consider (3), which we define as the COT problem, and analyze it.

Now the key challenge is that the conditionals $s(y/x), t(y/x)$ are not explicitly given, and only samples from the joints are available. Accordingly, we make an important decision by choosing an expected MMD-based regularizer for matching the conditionals:

$$\begin{aligned} & \min_{\pi: \mathcal{X} \mapsto \mathcal{P}(\mathcal{Y} \times \mathcal{Y})} \int_{\mathcal{X}} \int_{\mathcal{Y} \times \mathcal{Y}} c \, d\pi(x) da, \text{ s.t. } \int_{\mathcal{X}} \text{MMD}^2(\pi_1(x), s(y/x)) \, ds(x) \leq \epsilon_1, \\ & \int_{\mathcal{X}} \text{MMD}^2(\pi_2(x), t(y/x)) \, dt(x) \leq \epsilon_2. \end{aligned} \quad (4)$$

Note that (4) is same as (3) as $\epsilon_1, \epsilon_2 \rightarrow 0$ and whenever $s(x), t(x)$ are supported over entire \mathcal{X} . This is because MMD, being a metric, is always non-negative. Further, we employ a related kernel-regression based regularizer that finally enables us to overcome the challenge of conditionals being implicitly defined through the joint's samples:

$$\begin{aligned} & \min_{\pi: \mathcal{X} \mapsto \mathcal{P}(\mathcal{Y} \times \mathcal{Y})} \int_{\mathcal{X}} \int_{\mathcal{Y} \times \mathcal{Y}} c \, d\pi(x) da, \text{ s.t. } \int_{\mathcal{X} \times \mathcal{Y}} \text{MMD}^2(\pi_1(x), \delta_y) \, ds(x, y) \leq \epsilon_1 + \rho_1, \\ & \int_{\mathcal{X} \times \mathcal{Y}} \text{MMD}^2(\pi_2(x), \delta_y) \, dt(x, y) \leq \epsilon_2 + \rho_2. \end{aligned} \quad (5)$$

Here, $\rho_1 \equiv \int_{\mathcal{X} \times \mathcal{Y}} \text{MMD}^2(s(y/x), \delta_y) ds(x, y)$, $\rho_2 \equiv \int_{\mathcal{X} \times \mathcal{Y}} \text{MMD}^2(t(y/x), \delta_y) dt(x, y)$ and δ_y is the Dirac measure centred at y . From Theorem 3.1 in [Grünewälder et al., 2012] we have that (5) is same as (4) as $\epsilon_1, \epsilon_2 \rightarrow 0$. Now, for ease of optimization, we consider the Tikhonov regularized version:

$$\begin{aligned} \min_{\pi: \mathcal{X} \rightarrow \mathcal{P}(\mathcal{Y} \times \mathcal{Y})} \int_{\mathcal{X}} \int_{\mathcal{Y} \times \mathcal{Y}} c d\pi(x) da + \lambda_1 \int_{\mathcal{X} \times \mathcal{Y}} \text{MMD}^2(\pi_1(x), \delta_y) ds(x, y) \\ + \lambda_2 \int_{\mathcal{X} \times \mathcal{Y}} \text{MMD}^2(\pi_2(x), \delta_y) dt(x, y). \end{aligned} \quad (6)$$

where $\lambda_1, \lambda_2 > 0$ are regularization hyperparameters. We again note that our formulation (6) is a (valid) regularized version of the original conditional optimal transport problem (3) and (6) is same as (3) as $\lambda_1, \lambda_2 \rightarrow \infty$.

In our set-up, in order to solve (6) and perform estimation, we are only provided with samples $\mathcal{D}_m^s = \{(x_1, y_1), \dots, (x_m, y_m)\}$ and $\mathcal{D}_m^t = \{(x'_1, y'_1), \dots, (x'_m, y'_m)\}$ from $s(x, y), t(x, y)$ respectively. Hence we employ a sample-based estimator for the regularizer terms: $\int_{\mathcal{X} \times \mathcal{Y}} \text{MMD}^2(\pi_1(x), \delta_y) ds(x, y) \approx \frac{1}{m} \sum_{i=1}^m \text{MMD}^2(\pi_1(x_i), \delta_{y_i})$. The following lemma shows that this estimator is statistically consistent:

Lemma 1. *Assuming k is a normalized characteristic kernel, with probability atleast $1 - \delta$, we have:*

$$\left| \int_{\mathcal{X} \times \mathcal{Y}} \text{MMD}^2(\pi_1(x), \delta_y) ds(x, y) - \frac{1}{m} \sum_{i=1}^m \text{MMD}^2(\pi_1(x_i), \delta_{y_i}) \right| \leq 2\sqrt{\frac{2}{m} \log\left(\frac{2}{\delta}\right)}.$$

Using this result for the regularization terms, (6) can in-turn be estimated as:

$$\min_{\pi: \mathcal{X} \rightarrow \mathcal{P}(\mathcal{Y} \times \mathcal{Y})} \int_{\mathcal{X}} \int_{\mathcal{Y} \times \mathcal{Y}} c d\pi(x) da + \lambda_1 \frac{1}{m} \sum_{i=1}^m \text{MMD}^2(\pi_1(x_i), \delta_{y_i}) + \lambda_2 \frac{1}{m} \sum_{i=1}^m \text{MMD}^2(\pi_2(x'_i), \delta_{y'_i}). \quad (7)$$

Note that since a is a known distribution, we are not estimating it as an average over samples. In the following theorem, we prove the statistical consistency of (7).

Theorem 1. *Let $\hat{\mathcal{U}}_m[\pi], \mathcal{U}[\pi]$ denote the objectives in (7), (6) respectively. Let $\hat{\pi}_m, \pi^*$ denote their optimal solutions respectively. Then, the following statements are true:*

1. $\{\mathcal{U}[\hat{\pi}_m]\} \xrightarrow[p]{m \rightarrow \infty} \mathcal{U}[\pi^*]$ (converges in probability) whenever $TV(\hat{s}_m(x, y), s(x, y)) \xrightarrow{m \rightarrow \infty} 0$ and $TV(\hat{t}_m(x, y), t(x, y)) \xrightarrow{m \rightarrow \infty} 0$. Here, \hat{s}_m, \hat{t}_m denote the empirical measures corresponding to $\mathcal{D}_m^s, \mathcal{D}_m^t$. Under the same conditions, $\{\hat{\mathcal{U}}_m[\hat{\pi}_m]\} \xrightarrow[p]{m \rightarrow \infty} \mathcal{U}[\pi^*]$.
2. When π is restricted to some convenient class, say Π , learning bounds can be obtained: with probability atleast $1 - \delta$, $\mathcal{U}[\hat{\pi}_m] - \mathcal{U}[\pi^*] \leq 2(\lambda_1 + \lambda_2) \left(\mathcal{R}_m(\Pi) + 3\sqrt{\frac{1}{2m} \log\left(\frac{3}{\delta}\right)} \right)$. The Rademacher complexity term, \mathcal{R}_m , is defined and analyzed in Appendix 7.2. Also, with probability atleast $1 - \delta$, $|\hat{\mathcal{U}}_m[\hat{\pi}_m] - \mathcal{U}[\pi^*]| \leq 2(\lambda_1 + \lambda_2) \left(\mathcal{R}_m(\Pi) + 2\sqrt{\frac{1}{2m} \log\left(\frac{1}{\delta}\right)} \right)$.

We now provide details of modelling the transport plan function, i.e., choices for Π , from a pragmatic perspective. Firstly, we model the transport plan $\pi(y, y'/x)$ by modelling its factors: $\pi(y'/y, x)$ and $\pi(y/x)$. Since the factors can be modelled using simpler models, this brings us computational benefits among other advantages. Employing COT with such a factorization enables us to directly choose $\pi(y/x)$ as the label posterior of the model to be learnt in discriminative modelling applications. Also, the other factor $\pi(y'/y, x)$ can be readily used for inference (see sections 4.1.1, 4.3).

Transport plan with explicit models: Here, we assume $\mathcal{Y} = \{l_1, \dots, l_n\}$ is a finite set. Accordingly, we model the factors $\pi(y'/y, x), \pi(y/x)$ as neural networks with the output layer as softmax over the $|\mathcal{Y}| = n$ labels. The COT estimator 7 in this case simplifies as:

$$\begin{aligned} \min_{\psi, \theta} \int_{\mathcal{X}} \sum_{i=1, j=1}^{i=n, j=n} c(l_i, l_j) \pi_{\psi}(l_i/l_j, x) \pi_{\theta}(l_j/x) da(x) + \lambda_1 \frac{1}{m} \sum_{i=1}^m \text{MMD}^2 \left(\sum_{j=1}^n \pi_{\psi}(l_i/l_j, x_i) \pi_{\theta}(l_j/x_i), \delta_{y_i} \right) \\ + \lambda_2 \frac{1}{m} \sum_{i=1}^m \text{MMD}^2(\pi_{\theta}(l_i/x'_i), \delta_{y'_i}), \end{aligned} \quad (8)$$

where ψ, θ are the network parameters we wish to learn.

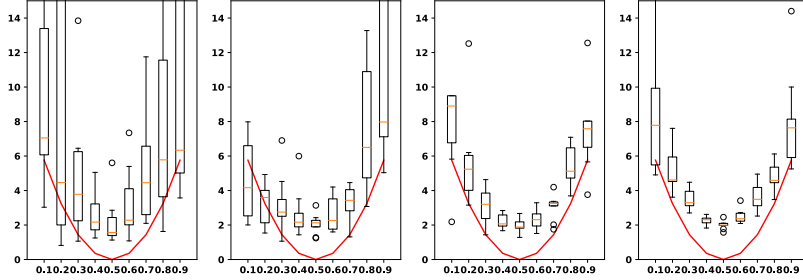


Figure 1: m , the number of training samples varies between $\{50, 100, 200, 400\}$ from left to right. The true Wasserstein distance is plotted in red color, and the estimated distances using our proposed estimator are marked in orange. The corresponding values of MSE $\{98.238, 18.476, 20.950, 6.995\}$.

Transport plan with implicit models: Here we consider the case where \mathcal{Y} is uncountable and the variable y is continuous. Implicit models that can generate samples are better suited for this scenario as it is then easy to estimate the expectations involved. Note that the MMD metric is meaningful even for distributions with potentially non-overlapping support. Thus the MMD-based regularization in COT naturally allows us to employ implicit models for the factors of the transport plan. The COT estimator, in this case, reads as:

$$\begin{aligned} \min_{\theta, \psi} \int_{\mathcal{X}} \frac{1}{m} \sum_{i=1}^m c(y_i(x; \theta), y_i(x; \theta, \psi)) da(x) + \lambda_1 \frac{1}{m} \sum_{i=1}^m \text{MMD}^2 \left(\frac{1}{m} \sum_{j=1}^m \delta_{y_j(x_i; \theta, \psi)}, \delta_{y_i} \right) \\ + \lambda_2 \frac{1}{m} \sum_{i=1}^m \text{MMD}^2 \left(\frac{1}{m} \sum_{j=1}^m \delta_{y_j(x'_i; \theta)}, \delta_{y'_i} \right), \end{aligned} \quad (9)$$

where $y_i(x; \theta) \ i = 1, \dots, m$ are samples from the network $\pi_{\theta}(\cdot/x)$ and $y_i(x; \theta, \psi) \ i = 1, \dots, m$ are samples from the network $\pi_{\psi}(\cdot/y_i(x; \theta), x)$.

4 Experiments

In this section, we showcase the utility of the proposed estimator 6 in various applications. We use $\lambda_1 = \lambda_2 = \lambda$ in all our experiments.

4.1 Verifying Correctness of Estimator

In case $a \sim \delta_{x_0}$ and λ_1, λ_2 are high enough, the transport cost term (first term) in (8)/(9) estimates $W_c(s(y/x_0), t(y/x_0))$. In order to verify this, we consider a case where the analytical solution for the Wasserstein distance W_c is known and compare it with our estimate.

Experiment setup We consider two distributions $y \sim \mathcal{N}(2(x - 0.5), 1)$ and $y' \sim \mathcal{N}(-4(x' - 0.5), 1)$ where $x \sim \beta(2, 4)$ and $x' \sim \beta(4, 2)$ generate m samples from each them. The true Wasserstein distance between them at x turns out to be $(6(x - 0.5))^2$ (see eqn (2.39) in [Peyré and Cuturi, 2020]). We use two 3 Layer MLP networks to model the factors $\pi_{\theta}(y/x)$ and $\pi_{\psi}(y'/y, x)$. We use RBF as our kernel and l_2 as our ground cost.

Results As shown in Figure 1 and the MSE values, the deviation between the empirical and variance decreases as the number of samples increases. Also, the variance of the estimated values decreases. More importantly, the shape of the function (quadratic) is more or less mimicked with our estimator.

4.1.1 Barycenter Experiment

For further verification of our estimator, we show that the barycenter estimated using our transport plan and the true barycenter converge in Wasserstein distance.

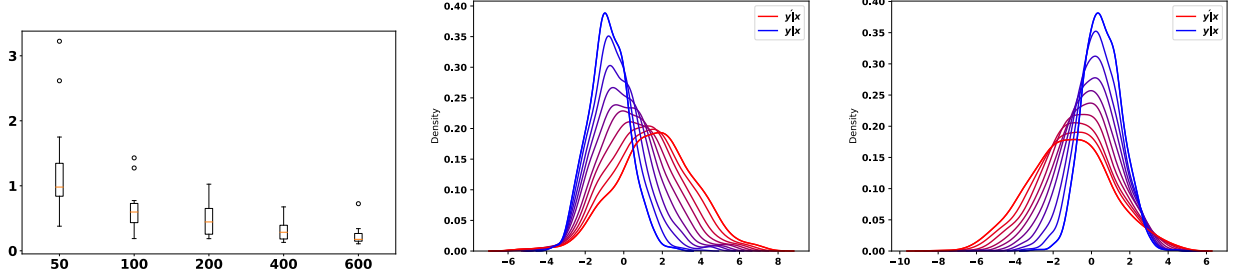


Figure 2: $W_c(B_x, \mathcal{N}(-x + 0.5, 2.5))$ for different values of m and a depiction of barycenter, B_x , for $x = 0.1$ and 0.8 with varying λ

Experiment setup: Two Independent Gaussian distributions are taken $y \sim \mathcal{N}(2(x - 0.5), 1)$ and $y' \sim \mathcal{N}(-4(x' - 0.5), 4)$ where $x \sim \beta(2, 4)$ and $x' \sim \beta(4, 2)$. The analytical solution of the barycenter is calculated as $y_c \sim \mathcal{N}(-x + 0.5, 2.5)$ [Peyré and Cuturi, 2020]. Recall that the barycenter can also be computed using the optimal transport plan using the expression: $B_x = \lambda S_x + (1 - \lambda)T_x$, where B_x, S_x denote the random variables corresponding to the barycenter and source measure conditioned at x . T_x 's distribution is $\pi(y'/x, S_x)$. Accordingly, samples from the barycenter, B_{x_i} , are obtained using: $\lambda y_i + (1 - \lambda)y$, where y is sampled from $\pi(\cdot/x_i, y_i)$.

Evaluation Protocol: For evaluation, we generate 500 samples from our transport plan based barycenter and the true barycenter. We plot the Wasserstein distance between these two as a function of the training set size, m .

Results: Figure 2 shows that the estimate of barycenter using our transport plan becomes better with m and is close enough for $m = 600$.

4.2 Classification

Since we can efficiently estimate the Wasserstein distance between conditionals solely from samples of joints, (7) can be used as a loss function in the supervised learning of discriminative models. The key advantage of using Wasserstein as a loss function is the fact that the Wasserstein metric lifts the geometry defined by the ground metric, $c : \mathcal{Y} \times \mathcal{Y} \mapsto \mathbb{R}$, to that between measures in $\mathcal{P}(\mathcal{Y})$.

COT based Classifier Let the discriminative model to be learnt be f_θ . The idea is to match this conditional to that in the training data using COT. We choose the transport plan factor $\pi_\theta \equiv f_\theta$ and a as the marginal of input covariates in the training data, simplifying our COT estimator, (8), as:

$$\min_{\psi, \theta} \frac{1}{m} \sum_{q=1}^m \sum_{i=1, j=1}^{i=n, j=n} c(l_i, l_j) \pi_\psi(l_i/l_j, x_q) f_\theta(l_j/x_q) + \lambda_1 \frac{1}{m} \sum_{i=1}^m \text{MMD}^2 \left(\sum_{j=1}^n \pi_\psi(l_i/l_j, x_i) f_\theta(l_j/x_i), \delta_{y_i} \right),$$

where ψ, θ are the network parameters we wish to learn. Note that we do not have the second MMD regularizer term as we directly choose $\pi_\theta \equiv f_\theta$. From the technical discussion in Section 3, this formulation can be understood as estimator for: $\min_\theta \mathbb{E}_{X \sim a} [W_c(f_\theta(y/X), s(y/X))]$.

Experimental setup We consider the task of multi-class classification and experiment on three benchmark datasets MNIST [LeCun and Cortes, 2010], CIFAR-10 [Krizhevsky et al., 2009] and Animals with Attribute (AWA) [Lampert et al., 2009]. We compare the performance of COT against entropy regularized Wasserstein (ϵ -OT) based loss as in [Frogner et al., 2015] and the standard cross entropy (CE) loss for classification. Following the popular approaches of minibatch OT [Fratras et al., 2020, Fratas et al., 2021], we train f_θ with COT loss in a minibatch fashion over the covariates. We use the implementation of [Frogner et al., 2015] open-sourced by [Jawanpuria et al., 2021]. We maintain the same experimental setup as used in [Jawanpuria et al., 2021]. The classifier is a single-layer neural network with Softmax activation which is trained for 200 epochs. We use the cost function, c , between labels as the squared l_2 distance between the fastText embeddings [Bojanowski et al., 2017] of the labels. The kernel function used in COT is $k(x, y) = e^{-\frac{c(x, y)}{2\sigma^2}}$. We use SGD with a learning rate of 0.1 and weight decay of 5×10^{-4} for optimization. For MNIST and CIFAR-10, we use the standard splits for training and testing and choose a random subset of size 10,000 from the training set for validation. For AWA, we use the train and test splits provided by [Jawanpuria et al., 2021] and randomly take 30% of the training data for validation.

Evaluation protocol Following [Jawanpuria et al., 2021], we compare all methods using the Area Under Curve (AUC) score of the classifier on the test data after finding the best hyperparameters on the validation data. Based on the validation phase, the best Sinkhorn regularization hyperparameter in ϵ -OT [Frogner et al., 2015] is 0.2. For COT, we choose the hyperparameters λ, σ based on the validation set: for MNIST and CIFAR-10, we find $\lambda = 0.1, \sigma^2 = 0.1$ and for AWA, we find $\lambda = 30, \sigma^2 = 1$ to be optimal.

Results As shown in Table 2, the classifier trained with the COT formulation consistently outperforms the classifier trained with ϵ -OT. The AUC scores with the proposed formulation also match that of the AUC scores with the popular cross entropy (CE) loss. We further compare the t-SNE of the representations learned by the models trained with COT and CE. We plot the t-SNE of the model representations for MNIST test data. The t-SNE plot 4.2 shows better-separated clusters (regions with a specific colour) corresponding to each class in the case of COT compared to the one obtained with CE, where the number of clusters is more than the number of classes in MNIST. The improved t-SNE plot can be attributed to the fact that the COT-based loss respects the geometry defined by the ground metric over the labels.

Dataset	CE	ϵ -OT	COT
MNIST	0.99	0.89	0.99
AWA	0.90	0.68	0.91
CIFAR10	0.78	0.66	0.79

Table 2: AUC on test data (higher is better)

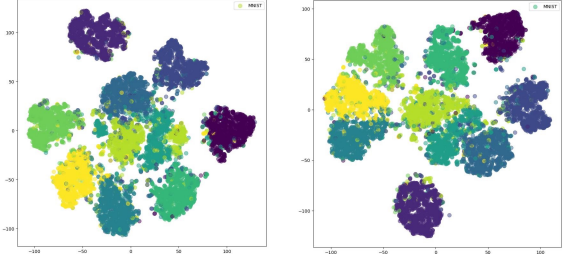


Figure 3: (Best viewed in colour) t-SNE Plots on MNIST test data with CE (left), COT (right).

4.3 Cell Population Dynamics

Problem Description The study of single-cell population dynamics is especially useful in studying the effect of drug dosages in medical applications. However, the current techniques for observing the gene expressions of the cells does so by destroying them. One often has unpaired distributions between control (unperturbed) cells and the cells treated with particular drug dosage. We apply our COT formulation to generate samples from perturbed distributions conditioned on the drug dosage given to an unperturbed cell.

Dataset We consider the dataset used by [Bunne et al., 2022] and [Bunne et al., 2021a] corresponding to the anti-cancer drug Givinostat applied at different dosage levels, $\{x_1 = 10nM, x_2 = 100nM, x_3 = 1000nM, x_4 = 10000nM\}$. At each dosage level, x_i , samples of perturbed cells are given: y_{i1}, \dots, y_{im_i} . The total perturbed cells are 3541. Samples of unperturbed cells are also provided: $y'_1, \dots, y'_m, m = 17, 565$. Each of these cells is described by gene-expression levels of $n = 1000$ highly variable genes i.e., $y_{ij}, y'_i \in \mathbb{R}^{1000}$.

COT-based Generative Modeling Our goal is to perform OT between the distribution of the unperturbed cells and the distribution of the perturbed cell conditioned on the drug dosage. Since $\mathcal{Y} = \mathbb{R}^{1000}$, we employ the implicit model based COT estimator for this purpose. We choose the implicit transport factor π_θ as the empirical distribution of unperturbed cells itself. With this notation and auxiliary a as the empirical distribution of the dosage levels, our COT estimator, (9), reads as:

$$\min_{\psi} \frac{1}{4} \sum_{q=1}^4 \frac{1}{m} \sum_{i=1}^m c(y'_i, y_i(x_q; \psi)) + \lambda_1 \frac{1}{4} \sum_{i=1}^4 \text{MMD}^2 \left(\frac{1}{m} \sum_{j=1}^m \delta_{y_j(x_i; \psi)}, \frac{1}{m_i} \sum_{j=1}^{m_i} \delta_{y_{ij}} \right),$$

where $y_i(x; \psi)$ $i = 1, \dots, m$ are samples from the network $\pi_\psi(\cdot/y'_i, x)$.

Experimental setup Similar to [Bunne et al., 2022], we take the cost function, c , as squared Euclidean. For the MMD regularization, we use the characteristic inverse multi-quadratic (IMQ) kernel, $k(x, y) = (h^2 + \|x - y\|^2)^{-1/2}$ kernel with the hyperparameter $h^2 = 10$. For each dosage level, we split the data into 80% for train and 20% for testing and report results on the test set.

Evaluation protocol Following [Bunne et al., 2022], we evaluate the performance on COT by comparing samples from the predicted and ground truth perturbed distributions. We report the l_2 norm between the Perturbation

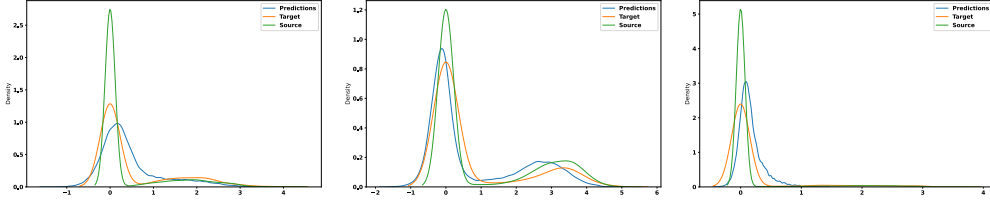


Figure 4: Marginals for selected genes ‘ENSG00000175175.5’, ‘ENSG00000173727.12’, ‘ENSG00000165092.12’ where the dosage is 100nM.

Table 3: l_2 (PS) distances between predicted and ground truth distributions

Method	$l_2(\text{PS})$
CPA	2.47 ± 2.89
ICNN	2.37 ± 2.15
CondOT	0.63 ± 0.09
CondOT	0.60 ± 0.11
COT	0.60 ± 0.11

Signatures [Stathias et al., 2018] for 50 marker genes for various dosage levels. The distances are reported for in-sample settings. We compare our performance to reported scores for various baselines CPA [Lotfollahi et al., 2021], ICNN [Makkuva et al., 2020] and CondOT [Bunne et al., 2022].

Results We summarize our obtained results in Table 3. We observe that COT outperforms earlier baselines such as CPA [Lotfollahi et al., 2021] and vanilla ICNN [Makkuva et al., 2020] approaches followed by CellOT [Bunne et al., 2021b]. Our formulation closely matches the performance of [Bunne et al., 2022]. However, [Bunne et al., 2022] are restricted to squared Euclidean cost, while our formulation is applicable for any cost metric, thus making it more generalizable over various applications.

4.4 Prompt Learning

In order to show the versatility of our framework, we adapt our estimator for learning prompts for large-scale vision-language models and evaluate the performance in limited supervision setting to show its usefulness for downstream tasks.

The success of vision-language models in open-world visual understanding has motivated efforts which aim to learn prompts [Zhou et al., 2022a, Zhang et al., 2021, Zhou et al., 2022b, Chen et al., 2023] to adapt the knowledge from pre-trained models like clip for downstream tasks since it is infeasible to fine-tune such models due to a large number of parameters. Typically, these approaches rely on learning class-specific prompts for each category to better adapt the vision-language model for downstream tasks without the need for fine-tuning. A recent approach, PLOT [Chen et al., 2023], proposes to learn a set of prompts by minimizing an OT-based loss between distributions over the set of local visual features and the set of textual prompt features, to learn the downstream classifier. For each image, PLOT computes an OT-based loss between $M(49)$ visual features of the image and $N(2)$ textual prompt features per class. As prompts are learnt on a per-class basis, we propose solving the COT problem by incorporating class-level information.

COT Formulation We learn an explicit model $\pi_{\psi_r}(l_{ir}/l_{jqr}, x_{qr})$ over the N textual prompt features l_{1r}, \dots, l_{Nr} for each class. Here, x_{qr} is the q^{th} image from class r and l_{jqr} is the j^{th} visual feature for image x_{qr} . In the K -shot classification setup, we have K images per class. Our formulation for prompt learning is as follows.

$$\min_{\psi_r} \frac{1}{K} \sum_{q=1}^K \sum_{i=1, j=1}^{i=N, j=M} c(l_{ir}, l_{jqr}) \pi_{\psi_r}(l_{ir}/l_{jqr}, x_{qr}) \mathbf{v}_j + \lambda_1 \text{MMD}^2 \left(\sum_{q=1}^K \sum_{j=1}^M \pi_{\psi_r}(\cdot/l_{jqr}, x_{qr}) \mathbf{v}_j, \mathbf{u} \right).$$

Following the PLOT setup, we take \mathbf{v}, \mathbf{u} are uniform distributions over the M visual features and the N prompt features respectively. Our formulation learns a transport plan conditioned on the image but matches the marginals of the plan at a class-level to incorporate the per-class distribution over prompts.

Table 4: Prompt Learning experiment: Average accuracy (higher is better) on EuroSAT dataset

	$K = 2$	$K = 4$	$K = 8$	$K = 16$
PLOT	64.21	71.80	77.90	82.30
COT	65.13	72.23	78.10	83.30

Experimental setup We follow the same experimental setup used in CoOP and PLOT for learning prompts and evaluate the performance of our method on the K -shot classification task. We report the performance (i.e accuracy) on the EuroSAT benchmark dataset [Helber et al., 2019] for 2, 4, 8 and 16 shots setting. Following PLOT, we use the cost function, $c(x, y) = 1 - x^\top y$. For computing MMD, we use the characteristic Dirac kernel $k(x, y) = \mathbb{I}[x = y]$. We follow the model architectures and common training/evaluation protocol used in CLIP, CoOP and PLOT and report average performance over 3 different seeds. **Results** Table 4 shows that COT achieves better average accuracy than PLOT.

5 Discussion and conclusion

Often machine learning applications need to compare conditional distributions. Remarkably, our framework enables such a comparison solely using samples from (observational) joint distributions. In this setting, we present consistent estimators for the optimal transport cost and plan between the conditionals. We discuss how our framework can be employed in diverse applications and in OT-style problems beyond COT.

6 Broader Impact

We believe our framework can have broader implications than described in this work. We speculate our methodology may be useful for conditional two-sample, conditional independence hypothesis testing, handling covariate shift, manifold-valued discriminative/conditional-generative models etc. When used as a loss function, our training is an alternative to the popular MLE estimation in discriminative models. The advantage being that the loss function is domain-geometric-aware, unlike the KL-divergence.

7 Supplementary Materials

7.1 Proof of Lemma 1

Lemma1. Assuming k is a normalized characteristic kernel, with probability atleast $1 - \delta$, we have:

$$\left| \int_{\mathcal{X} \times \mathcal{Y}} \text{MMD}^2(\pi_1(x), \delta_y) \text{d}s(x, y) - \frac{1}{m} \sum_{i=1}^m \text{MMD}^2(\pi_1(x_i), \delta_{y_i}) \right| \leq 2\sqrt{\frac{2}{m} \log\left(\frac{2}{\delta}\right)}.$$

Proof. Recall that MMD is nothing but the RKHS norm-induced distance between the corresponding kernel embeddings i.e., $\text{MMD}(s, t) = \|\mu_k(s) - \mu_k(t)\|$, where $\mu_k(s) \equiv \int \phi_k(x) \text{d}s(x)$, is the kernel mean embedding of s [Muandet et al., 2017], ϕ_k is the canonical feature map associated with the characteristic kernel k . Let \mathcal{H}_k denote the RKHS associated with the kernel k . Since our kernel is normalized we have that $\|\mu_k(b)\| \leq 1 \forall b \in \mathcal{P}(\mathcal{Y})$. Hence, $0 \leq \text{MMD}^2(\pi_1(x), s(y/x)) \leq 4$. From Chernoff-Hoeffding bound, we have that: with probability atleast $1 - \delta$, $\left| \int_{\mathcal{X} \times \mathcal{Y}} \text{MMD}^2(\pi_1(x), \delta_y) \text{d}s(x, y) - \frac{1}{m} \sum_{i=1}^m \text{MMD}^2(\pi_1(x_i), \delta_{y_i}) \right| \leq 2\sqrt{\frac{2}{m} \log\left(\frac{2}{\delta}\right)}$. \square

7.2 Proof of Theorem 1

Theorem1. Let $\hat{\mathcal{U}}_m[\pi], \mathcal{U}[\pi]$ denote the objectives in (7), (6) respectively. Let $\hat{\pi}_m, \pi^*$ denote their optimal solutions respectively. Then, the following statements are true:

1. $\{\mathcal{U}[\hat{\pi}_m]\} \xrightarrow[p]{m \rightarrow \infty} \mathcal{U}[\pi^*]$ (converges in probability) whenever $TV(\hat{s}_m(x, y), s(x, y)) \xrightarrow{m \rightarrow \infty} 0$ and $TV(\hat{t}_m(x, y), t(x, y)) \xrightarrow{m \rightarrow \infty} 0$. Here, \hat{s}_m, \hat{t}_m denote the empirical measures corresponding to $\mathcal{D}_m^s, \mathcal{D}_m^t$. Under the same conditions, $\{\hat{\mathcal{U}}_m[\hat{\pi}_m]\} \xrightarrow[p]{m \rightarrow \infty} \mathcal{U}[\pi^*]$.

2. When π is restricted to some convenient class, say Π , learning bounds can be obtained: with probability at least $1 - \delta$, $\mathcal{U}[\hat{\pi}_m] - \mathcal{U}[\pi^*] \leq 2(\lambda_1 + \lambda_2) \left(\mathcal{R}_m(\Pi) + 3\sqrt{\frac{1}{2m} \log\left(\frac{3}{\delta}\right)} \right)$. The Rademacher complexity term, \mathcal{R}_m , is defined and analyzed in Appendix 7.2. Also, with probability at least $1 - \delta$, $\left| \hat{\mathcal{U}}_m[\hat{\pi}_m] - \mathcal{U}[\pi^*] \right| \leq 2(\lambda_1 + \lambda_2) \left(\mathcal{R}_m(\Pi) + 2\sqrt{\frac{1}{2m} \log\left(\frac{1}{\delta}\right)} \right)$.

Proof. We begin by recalling that

$$\hat{\mathcal{U}}_m[\pi] \equiv \int_{\mathcal{X}} \int_{\mathcal{Y} \times \mathcal{Y}} c \, d\pi(x) da + \lambda_1 \frac{1}{m} \sum_{i=1}^m \text{MMD}^2(\pi_1(x_i), \delta_{y_i}) + \lambda_2 \frac{1}{m} \sum_{i=1}^m \text{MMD}^2(\pi_2(x'_i), \delta_{y'_i})$$

is the objective in 7 and $\hat{\pi}_m$ is the corresponding optimal solution.

Similarly,

$$\mathcal{U}[\pi] \equiv \int_{\mathcal{X}} \int_{\mathcal{Y} \times \mathcal{Y}} c \, d\pi(x) da + \lambda_1 \int_{\mathcal{X} \times \mathcal{Y}} \text{MMD}^2(\pi_1(x), \delta_y) \, ds(x, y) + \lambda_2 \int_{\mathcal{X} \times \mathcal{Y}} \text{MMD}^2(\pi_2(x), \delta_y) \, dt(x, y)$$

is the objective in 6 and π^* is the corresponding optimal solution.

It follows that $0 \leq \mathcal{U}[\hat{\pi}_m] - \mathcal{U}[\pi^*]$.

$$\begin{aligned} 0 \leq \mathcal{U}[\hat{\pi}_m] - \mathcal{U}[\pi^*] &= \mathcal{U}[\hat{\pi}_m] - \hat{\mathcal{U}}_m[\hat{\pi}_m] + \hat{\mathcal{U}}_m[\hat{\pi}_m] - \hat{\mathcal{U}}_m[\pi^*] + \hat{\mathcal{U}}_m[\pi^*] - \mathcal{U}[\pi^*] \\ &\leq \mathcal{U}[\hat{\pi}_m] - \hat{\mathcal{U}}_m[\hat{\pi}_m] + \hat{\mathcal{U}}_m[\pi^*] - \mathcal{U}[\pi^*] \quad (\because \hat{\pi}_m \text{ is the solution of 7}) \\ &\leq \max_{\pi: \mathcal{X} \mapsto \mathcal{P}(\mathcal{Y} \times \mathcal{Y})} (\mathcal{U}[\pi] - \hat{\mathcal{U}}_m[\pi]) + \hat{\mathcal{U}}_m[\pi^*] - \mathcal{U}[\pi^*] \end{aligned} \quad (10)$$

We now separately upper bound the two terms in 10: $(\hat{\mathcal{U}}_m[\pi^*] - \mathcal{U}[\pi^*])$ and $\max_{\pi: \mathcal{X} \mapsto \mathcal{P}(\mathcal{Y} \times \mathcal{Y})} (\mathcal{U}[\pi] - \hat{\mathcal{U}}_m[\pi])$. From Lemma 1, with probability at least $1 - \delta$,

$$\hat{\mathcal{U}}_m[\pi^*] - \mathcal{U}[\pi^*] \leq 2(\lambda_1 + \lambda_2) \sqrt{\frac{2}{m} \log \frac{2}{\delta}} \quad (11)$$

Proof of Theorem 1.1: We upper-bound the second term as follows.

$$\begin{aligned} \max_{\pi: \mathcal{X} \mapsto \mathcal{P}(\mathcal{Y} \times \mathcal{Y})} (\mathcal{U}[\pi] - \hat{\mathcal{U}}_m[\pi]) &\leq \left| \lambda_1 \left(\max_{\pi_1: \mathcal{X} \mapsto \mathcal{P}(\mathcal{Y})} \left(\int_{\mathcal{X} \times \mathcal{Y}} \text{MMD}^2(\pi_1(x), \delta_y) \, ds(x, y) - \int_{\mathcal{X} \times \mathcal{Y}} \text{MMD}^2(\pi_1(x), \delta_y) \, d\hat{s}_m(x, y) \right) \right) \right. \\ &\quad \left. + \lambda_2 \left(\max_{\pi_2: \mathcal{X} \mapsto \mathcal{P}(\mathcal{Y})} \left(\int_{\mathcal{X} \times \mathcal{Y}} \text{MMD}^2(\pi_2(x), \delta_y) \, dt(x, y) - \int_{\mathcal{X} \times \mathcal{Y}} \text{MMD}^2(\pi_2(x), \delta_y) \, d\hat{t}_m(x, y) \right) \right) \right| \\ &= \left| \lambda_1 \max_{\pi_1: \mathcal{X} \mapsto \mathcal{P}(\mathcal{Y})} \int_{\mathcal{X} \times \mathcal{Y}} \text{MMD}^2(\pi_1(x), \delta_y) \, d(s - \hat{s}_m)(x, y) \right. \\ &\quad \left. + \lambda_2 \max_{\pi_2: \mathcal{X} \mapsto \mathcal{P}(\mathcal{Y})} \int_{\mathcal{X} \times \mathcal{Y}} \text{MMD}^2(\pi_2(x), \delta_y) \, d(t - \hat{t}_m)(x, y) \right| \\ &\leq \lambda_1 \max_{\pi_1: \mathcal{X} \mapsto \mathcal{P}(\mathcal{Y})} \int_{\mathcal{X} \times \mathcal{Y}} \text{MMD}^2(\pi_1(x), \delta_y) \, d(|s - \hat{s}_m|)(x, y) \\ &\quad + \lambda_2 \max_{\pi_2: \mathcal{X} \mapsto \mathcal{P}(\mathcal{Y})} \int_{\mathcal{X} \times \mathcal{Y}} \text{MMD}^2(\pi_2(x), \delta_y) \, d(|t - \hat{t}_m|)(x, y) \\ &\quad \text{(Using triangle inequality)} \\ &\leq 4\lambda_1 \text{TV}(s, \hat{s}_m) + 4\lambda_2 \text{TV}(t, \hat{t}_m) \\ &\quad (\because \|\phi(\cdot)\| = 1, \|\mu_k(\cdot)\| \leq 1 \text{ with a normalized kernel, } k) \end{aligned} \quad (12)$$

Using inequalities 11 and 12 in inequality 10, we have that with probability atleast $1 - \delta$,

$$0 \leq \mathcal{U}[\hat{\pi}_m] - \mathcal{U}[\pi^*] \leq 2(\lambda_1 + \lambda_2) \sqrt{\frac{2}{m} \log \frac{2}{\delta}} + 4(\lambda_1 \text{TV}(s, \hat{s}_m) + \lambda_2 \text{TV}(t, \hat{t}_m))$$

Hence, we proved that $\{\mathcal{U}[\hat{\pi}_m]\} \xrightarrow[p]{m \rightarrow \infty} \mathcal{U}[\pi^*]$ (converges in probability) whenever $\text{TV}(\hat{s}_m, s) \xrightarrow{m \rightarrow \infty} 0$ and $\text{TV}(\hat{t}_m, t) \xrightarrow{m \rightarrow \infty} 0$.

Further, $\hat{\mathcal{U}}_m[\hat{\pi}_m] - \mathcal{U}[\pi^*] = \hat{\mathcal{U}}_m[\hat{\pi}_m] - \mathcal{U}[\pi^*] - \hat{\mathcal{U}}_m[\pi^*] + \hat{\mathcal{U}}_m[\pi^*] \leq \max_{\pi: \mathcal{X} \rightarrow \mathcal{P}(\mathcal{Y} \times \mathcal{Y})} \hat{\mathcal{U}}_m[\pi] - \mathcal{U}[\pi]$. Also, $\mathcal{U}[\pi^*] - \hat{\mathcal{U}}_m[\hat{\pi}_m] = \mathcal{U}[\pi^*] - \hat{\mathcal{U}}_m[\hat{\pi}_m] - \mathcal{U}[\hat{\pi}_m] + \mathcal{U}[\hat{\pi}_m] \leq \max_{\pi: \mathcal{X} \rightarrow \mathcal{P}(\mathcal{Y} \times \mathcal{Y})} -\hat{\mathcal{U}}_m[\pi] + \mathcal{U}[\pi]$. It follows that $\{\hat{\mathcal{U}}_m[\hat{\pi}_m]\} \xrightarrow[p]{m \rightarrow \infty} \mathcal{U}[\pi^*]$ (converges in probability) under the same conditions.

Proof of Theorem 1.2: We first show that $\max_{\pi: \mathcal{X} \rightarrow \mathcal{P}(\mathcal{Y} \times \mathcal{Y})} \mathcal{U}[\pi] - \hat{\mathcal{U}}_m[\pi]$ satisfies the bounded difference property. Let Z_i denote the random variable (X_i, Y_i) . Let $Z = \{Z_1, \dots, Z_i, \dots, Z_m\}$ be a set of independent random variables. Consider another such set that differs only at the i^{th} position: $Z' = \{Z_1, \dots, Z_i', \dots, Z_m\}$. Let $\hat{\mathcal{U}}_m[\pi]$ and $\hat{\mathcal{U}}_m'[\pi]$ be the corresponding objectives in 7.

$$\begin{aligned} & \left| \max_{\pi: \mathcal{X} \rightarrow \mathcal{P}(\mathcal{Y} \times \mathcal{Y})} (\mathcal{U}[\pi] - \hat{\mathcal{U}}_m[\pi]) - \max_{\pi: \mathcal{X} \rightarrow \mathcal{P}(\mathcal{Y} \times \mathcal{Y})} (\mathcal{U}[\pi] - \hat{\mathcal{U}}_m'[\pi]) \right| \\ & \leq \left| \max_{\pi: \mathcal{X} \rightarrow \mathcal{P}(\mathcal{Y} \times \mathcal{Y})} -\hat{\mathcal{U}}_m[\pi] + \hat{\mathcal{U}}_m'[\pi] \right| \\ & \leq \frac{\lambda_1}{m} \left| \max_{\pi_1: \mathcal{X} \rightarrow \mathcal{P}(\mathcal{Y})} \text{MMD}^2(\pi_1(x_i), \delta_{y_i}) - \text{MMD}^2(\pi_1(x_i'), \delta_{y_i'}) \right| \\ & \quad + \frac{\lambda_2}{m} \left| \max_{\pi_2: \mathcal{X} \rightarrow \mathcal{P}(\mathcal{Y})} \text{MMD}^2(\pi_2(x_i), \delta_{y_i}) - \text{MMD}^2(\pi_2(x_i'), \delta_{y_i'}) \right| \\ & \text{(using triangle inequality)} \\ & \leq \frac{8(\lambda_1 + \lambda_2)}{m} \text{(with a normalized kernel based MMD)} \end{aligned} \quad (13)$$

Using the above in McDiarmid's inequality,

$$\max_{\pi: \mathcal{X} \rightarrow \mathcal{P}(\mathcal{Y} \times \mathcal{Y})} \mathcal{U}[\pi] - \hat{\mathcal{U}}_m[\pi] \leq \mathbb{E} \left[\max_{\pi: \mathcal{X} \rightarrow \mathcal{P}(\mathcal{Y} \times \mathcal{Y})} \mathcal{U}[\pi] - \hat{\mathcal{U}}_m[\pi] \right] + 4(\lambda_1 + \lambda_2) \sqrt{\frac{2}{m} \log \frac{1}{\delta}} \quad (14)$$

We begin with $\mathcal{D}_m = \{(x_1, y_1), \dots, (x_m, y_m)\}$ as an independent set of training data samples. We denote the random variable (X_i, Y_i) by Z_i and $Z = \{Z_1, \dots, Z_m\}$. Let $(\epsilon_i)_{i \in \{1, \dots, m\}}$ be IID Rademacher random variables. We now follow the standard symmetrization trick and introduce the Rademacher random variables to get the following.

$$\mathbb{E} \left[\max_{\pi: \mathcal{X} \rightarrow \mathcal{P}(\mathcal{Y} \times \mathcal{Y})} \mathcal{U}[\pi] - \hat{\mathcal{U}}_m[\pi] \right] \leq 2(\lambda_1 + \lambda_2) \mathbb{E}_{Z, \epsilon} \left[\max_{\pi_1: \mathcal{X} \rightarrow \mathcal{P}(\mathcal{Y})} \sum_{i=1}^m \frac{\epsilon_i}{m} \|\mu_k(\pi_1(X_i)) - \phi(Y_i)\|^2 \right] \quad (15)$$

Let $\Pi \subseteq \{\pi_1: \mathcal{X} \rightarrow \mathcal{P}(\mathcal{Y})\}$ be an appropriately restricted model for the conditional transport plan. Let $\mathcal{R}_m(\Pi) \equiv \mathbb{E} \left[\max_{\pi_1 \in \Pi} \sum_{i=1}^m \frac{\epsilon_i}{m} \|\mu_k(\pi_1(X_i)) - \phi(Y_i)\|^2 \right]$.

Hence, using 11, 14 and 15, we proved that with probability atleast $1 - \delta$,

$$\mathcal{U}[\hat{\pi}_m] - \mathcal{U}[\pi^*] \leq 2(\lambda_1 + \lambda_2) \left(\mathcal{R}_m(\Pi) + 3\sqrt{\frac{2}{m} \log \frac{3}{\delta}} \right). \quad (16)$$

Further, as shown in the previous part of the proof, we have that $\hat{\mathcal{U}}_m[\hat{\pi}_m] - \mathcal{U}[\pi^*] \leq \max_{\pi: \mathcal{X} \rightarrow \mathcal{P}(\mathcal{Y} \times \mathcal{Y})} \hat{\mathcal{U}}_m[\pi] - \mathcal{U}[\pi]$ and $\mathcal{U}[\pi^*] - \hat{\mathcal{U}}_m[\hat{\pi}_m] \leq \max_{\pi: \mathcal{X} \rightarrow \mathcal{P}(\mathcal{Y} \times \mathcal{Y})} -\hat{\mathcal{U}}_m[\pi] + \mathcal{U}[\pi]$. Thus, with probability atleast $1 - \delta$, $|\hat{\mathcal{U}}_m[\hat{\pi}_m] - \mathcal{U}[\pi^*]| \leq 2(\lambda_1 + \lambda_2) \left(\mathcal{R}_m(\Pi) + 2\sqrt{\frac{2}{m} \log \frac{2}{\delta}} \right)$.

Bounding Rademacher in a special case: We now upper-bound $\mathcal{R}_m(\Pi)$ for a special case where $\pi_1(x), \pi_2(x)$ are implicitly defined using (conditional) generative models, i.e., $g_w(x, N) \sim \pi_1(x)$, where g_w is a function parameterized

by \mathbf{w} (perhaps a neural network function). Let $\zeta_i(\pi_1) \equiv \|\mu_k(\pi_1(x_i)) - \phi(y_i)\|^2$. Denoting \mathcal{H}_k as the RKHS associated with characteristic kernel k and \mathcal{C} as the set of continuous functions and $\mathcal{W}_c = \{f : f \in \mathcal{C}; \|f\|_c \leq 1\}$, we have that,

$$\begin{aligned}
\zeta_i(\pi_1) - \zeta_i(\pi'_1) &\leq 4\|\mu_k(\pi_1(x_i)) - \mu_k(\pi'_1(x_i))\| \text{ (Using triangle inequality and boundedness of embeddings)} \\
&= 4 \max_{f \in \mathcal{H}_k; \|f\| \leq 1} \mathbb{E}[f(g_{\mathbf{w}}(x_i, N))] - \mathbb{E}[f(g_{\mathbf{w}'}(x_i, N'))] \text{ (Using dual norm definition of MMD)} \\
&\stackrel{(1)}{\leq} 4 \max_{f \in \mathcal{C}; \|f\|_c \leq 1} \mathbb{E}[f(g_{\mathbf{w}}(x_i, N))] - \mathbb{E}[f(g_{\mathbf{w}'}(x_i, N'))] \\
&= 4 \max_{f \in \mathcal{C}; \|f\|_c \leq 1} \int (f(g_{\mathbf{w}}(x_i, n)) - f(g_{\mathbf{w}'}(x_i, n))) \, dn \\
&\leq 4 \int c(g_{\mathbf{w}}(x_i, n), g_{\mathbf{w}'}(x_i, n)) \, dn \tag{17}
\end{aligned}$$

The last inequality follows from max-integral interchange and $\|f\|_c \leq 1$. Inequality (1) uses the following relation between MMD and 1-Wasserstein when the cost function involved is the kernel distance ($c(x, y) = \|\phi(x) - \phi(y)\|_{\mathcal{H}_k}$):

$$\begin{aligned}
\text{MMD}(s, t) &\stackrel{\text{def.}}{=} \max_{f \in \mathcal{H}_k; \|f\| \leq 1} |\mathbb{E}_s[f(X)] - \mathbb{E}_t[f(X)]| \\
W_1(s, t) &\stackrel{\text{def.}}{=} \max_{f \in \mathcal{C}; \|f\|_c \leq 1} |\mathbb{E}_s[f(X)] - \mathbb{E}_t[f(X)]|
\end{aligned}$$

Let $f \in \mathcal{H}_k$, $\|f\|_{\mathcal{H}_k} \leq 1$

$$\begin{aligned}
|f(x) - f(y)| &= |\langle f, \phi(x) - \phi(y) \rangle| \text{ (RKHS property)} \\
&\leq \|f\|_{\mathcal{H}_k} \|\phi(x) - \phi(y)\|_{\mathcal{H}_k^*} \text{ (Holders Inequality)} \\
&\leq \|\phi(x) - \phi(y)\|_{\mathcal{H}_k} (\because \|f\|_{\mathcal{H}_k} \leq 1) \\
&= c(x, y) \\
&\implies f \in \mathcal{W}_c \\
&\implies \text{MMD}(s, t) \leq W_1(s, t)
\end{aligned}$$

Now, to simplify the bounds, we further assume the Lipschitz continuity condition: $\|\phi(g_{\mathbf{w}}(x_i, n)) - \phi(g_{\mathbf{w}'}(x_i, n))\|_{\mathcal{H}_k} \leq L_i \|\mathbf{w} - \mathbf{w}'\|$. We present a special case for this to hold, as follows. Consider $g_{\mathbf{w}}(x_i, n) = \mathbf{M}(x_i, n)\mathbf{w}$ such that $\|\mathbf{M}(x_i, n)\mathbf{w}\| = 1$. Now, with the sufficient conditions derived in Section A.3 of [Manupriya et al., 2023], (i.e. using an RBF kernel $k(x, y) = \exp(-s\|x - y\|^2)$ with $s \in (0, 0.5]$), we have that $\|\phi(g_{\mathbf{w}}(x_i, n)) - \phi(g_{\mathbf{w}'}(x_i, n))\|_{\mathcal{H}_k} \leq \|g_{\mathbf{w}}(x_i, n) - g_{\mathbf{w}'}(x_i, n)\| \leq \sigma_{\max}(\mathbf{M}(x_i, n)) \|\mathbf{w} - \mathbf{w}'\|$.

With this, 17 implies that $\zeta_i(\cdot)$ is a $4L_i$ -Lipschitz continuous function. We also assume $\|\mathbf{w}\|_2 \leq 1$ (regularization of parameters). We next use Corollary (4) from [Maurer, 2016] with r_{ij} as an independent doubly indexed Rademacher

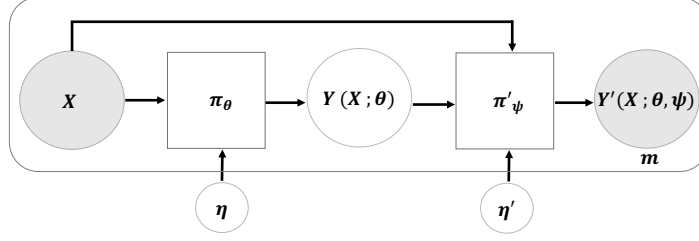


Figure 5: Illustration of the Implicit Model used

sequence.

$$\begin{aligned}
\mathcal{R}_m(\Pi) &\leq \frac{4\sqrt{2}}{m} \mathbb{E} \left[\max_{\|\mathbf{w}\| \leq 1} \sum_{i=1}^m L_i \mathbf{r}_i^\top \mathbf{w} \right] \\
&\text{(From Corollary (4) in [Maurer, 2016])} \\
&= \frac{4\sqrt{2}}{m} \mathbb{E} \left[\max_{\|\mathbf{w}\| \leq 1} \mathbf{w}^\top \left(\sum_{i=1}^m \mathbf{r}_i L_i \right) \right] \\
&\leq \frac{4\sqrt{2}}{m} \mathbb{E} \left[\left\| \sum_{i=1}^m \mathbf{r}_i L_i \right\|_2 \right] \text{ (using Cauchy Schwarz)} \\
&\leq \frac{4\sqrt{2}}{m} \sqrt{\mathbb{E} \left[\left\| \sum_{i=1}^m \mathbf{r}_i L_i \right\|_2^2 \right]} \text{ (Jensen's inequality)} \\
&= \frac{4\sqrt{2}}{m} \sqrt{\sum_{i=1}^m L_i^2} \text{ (using property of Rademacher variables)} \\
&\leq 4\sqrt{\frac{2}{m}} \text{ (if } L_i \leq 1). \\
&\rightarrow 0 \text{ as } m \rightarrow \infty.
\end{aligned} \tag{18}$$

Suppose λ grows as $O(m^{\frac{1}{4}})$, the estimation error would then decay as $O(m^{-\frac{1}{4}})$, making our estimator consistent. \square

7.3 More details on experiments

This section contains more experimental details along with some additional results.

7.3.1 Implicit modelling of the transport plan

In continuation to Section 3 in the main paper, we give more details on the implicit modelling approach for the COT transport plan. Figure 5 shows the implicit model used in our work. For inference, we pass different noise samples and average the outputs of π'_ψ .

Visualizing the predictions We take a synthetic regression data and show the predictions learnt by the implicit conditional generator trained with the COT loss 9. We fix λ to 500, noise dimension to 10. We use Adam optimizer with a learning rate $5e - 3$ and train for 1000 epochs. We use squared Euclidean distance and RBF kernel. Figure 6 shows that we obtain a good fit for $\sigma^2 = 10, 100$. For the same task, we also show the COT training objective over epochs in Figure 7.

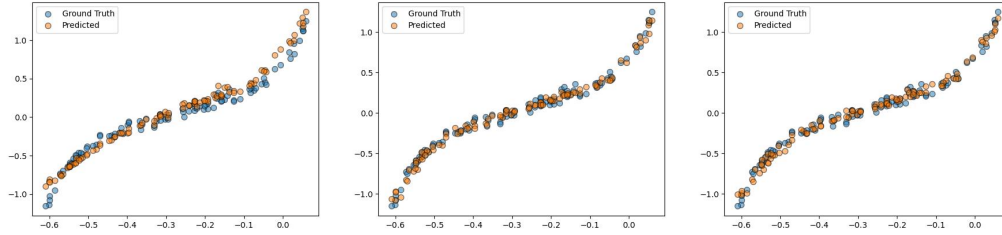


Figure 6: Predictions of the implicit conditional generator trained with the COT loss. The plots show the effect of different σ^2 hyperparameters used in the RBF kernel: 1 (left), 10 (center), 100 (right).

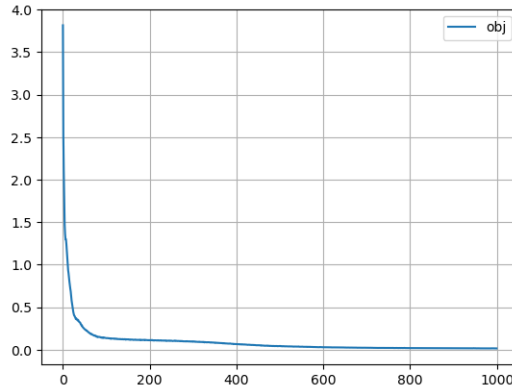


Figure 7: The COT objective over epochs curve while training the implicit conditional generator for the results shown in Figure 6

7.3.2 Verifying Correctness of Estimator

For the results shown in Figure 1 and Figure 2, we use $\lambda_1 = \lambda_2$ as 600; the noise dimension as 10, and the σ^2 hyperparameter in RBF kernel as 1. We use Adam optimizer with a learning rate $3e - 2$, weight decay $1e - 10$ and trained our implicit model for 1500 epochs.

7.3.3 Classification

We generate a 2D blob dataset for 3 classes having the number of samples as 300, 400 and 300. We divide it into train and test splits, maintaining the class ratio's in the two splits. In Figure 8, we first show the decision boundary of the untrained classifier on the test data. We then visualize the classifier's decision boundaries for different values of

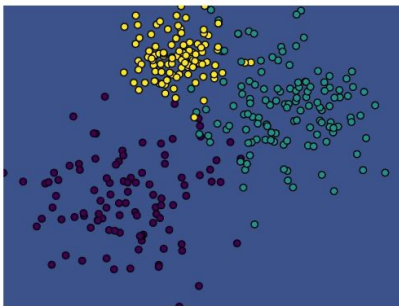


Figure 8: The test data points, colored according to class labels, are displayed along with the decision boundaries of the untrained classifier. It can be seen that the decision boundary of the untrained classifier is not able to classify points and the resulting test accuracy is 30%.

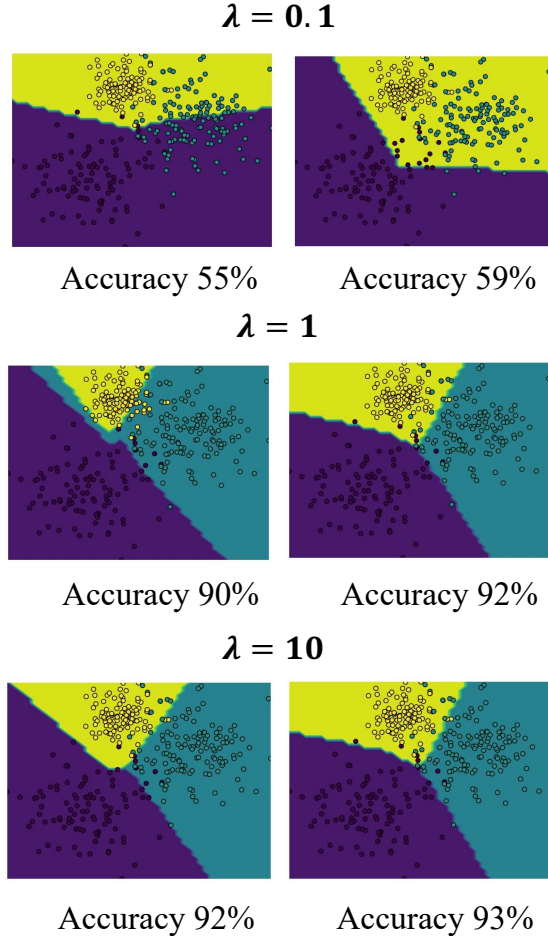


Figure 9: The test data points, colored according to class labels, are displayed along with the decision boundary of the classifier trained for 10 epochs (left column) and 50 epochs (right column).

Table 5: Per-epoch computation time with minibatch size (B)

B	Time (ms)
16	9.4
64	9.6
256	9.0
1024	9.1

λ in Figure 9 after training on the train split. For training, we use a batch size of 50 and the Adam optimizer with a learning rate of $5e - 3$. Due to the labels being discrete, our cost matrix, as well as Gram matrix, are Identity matrices for classification. Figure 8 shows that on increasing λ , the classifier learns with a lesser number of epochs showing the effect of MMD-based regularization used in the COT formulation.

In Table 5, we also show the per-epoch computation time taken (on an RTX 2080 Ti GPU) by the COT loss as a function of the size of the minibatch, which shows the computational efficiency of the COT loss.

7.3.4 Cell Population Dynamics

Dataset We use the preprocessed dataset provided by [Bunne et al., 2021a]. The dataset is publicly available for download using the following link

<https://polybox.ethz.ch/index.php/s/RAykIMfDl0qCJaM>.

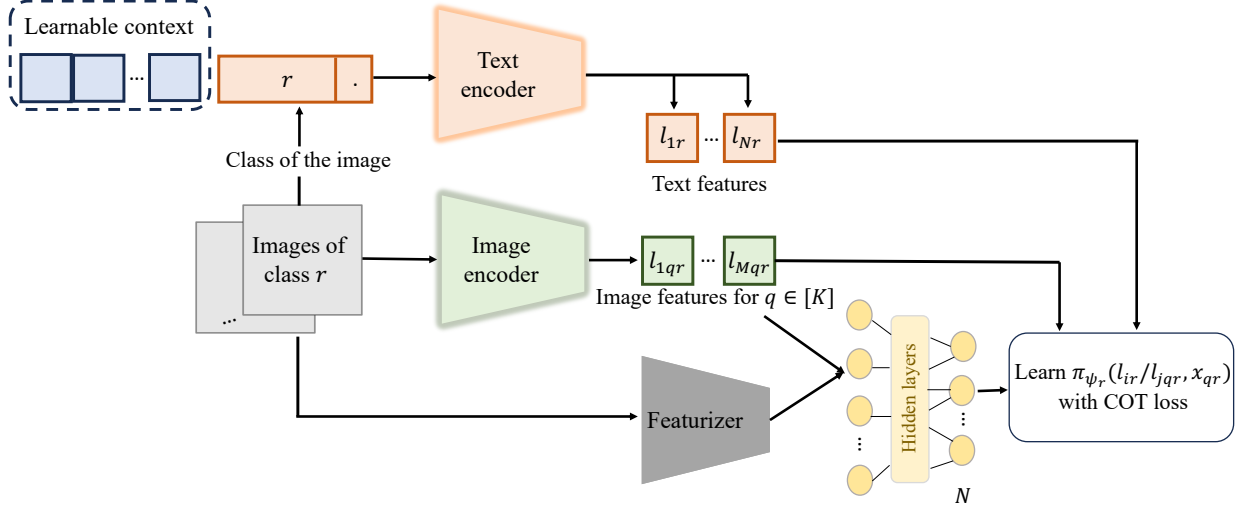


Figure 10: Learning the conditional transport plans for Prompt learning

From this dataset, we extracted unperturbed cells and cells treated with Givinostat. This led to a total of 17565 control cells, and a total of 3541 cells treated with Givinostat. We take the same data splits as in [Bunne et al., 2021a].

Marker Genes Following [Bunne et al., 2022], we use `scanny`'s [Wolf et al., 2018] `rank_genes_groups` function for ranking and obtaining 50 marker genes for each drug dosage. The perturbed cells are grouped by drug dosage and the ranking is computed by keeping the unperturbed (i.e. control) cells as reference. Similar to [Bunne et al., 2022], COT also operates on the entire 1000 genes, and the computed 50 marker genes are only used for evaluation using the $l_2(\mathbf{PS})$ metric.

Following the in-sample experiment done in [Bunne et al., 2022], we tune our hyperparameters on the training data split. Based on the scale of terms in the COT objective, we chose λ_1 from the set $\{250, 2500, 5000, 12500\}$ and found $\lambda_1 = 5000$ to be the optimal choice. For the IMQ kernel, we choose the hyperparameter from the set $\{1, 10, 100\}$ and found 10 to be the optimal choice. We fixed the noise dimension to 20. For all the experiments reported above, we used an MLP with 4 hidden layers, which was trained for 950 epochs. For inference used in Table 3, we average the outputs generated by our implicit network corresponding to 10 noise samples. For inference used in plotting the marginals shown in Figure 4, we average the outputs generated by our implicit network corresponding to 50 noise samples.

Following [Bunne et al., 2022], we quantitatively evaluate our performance using the l_2 distance between the perturbation signatures, $l_2(\mathbf{PS})$ metric. Let μ be the set of observed unperturbed cell population, ν be the set of the observed perturbed cell population (of size m_1), and ν' be the set of predicted perturbed state of population μ (of size m_2). The perturbation signature $\mathbf{PS}(\nu, \mu)$ is then defined as $\frac{1}{m_1} \sum_{y_i \in \nu} y_i - \frac{1}{m_2} \sum_{y_i \in \mu} y_i'$. The $l_2(\mathbf{PS})$ metric is the l_2 distance between $\mathbf{PS}(\nu, \mu)$ and $\mathbf{PS}(\hat{\nu}, \mu)$.

7.3.5 Prompt Learning

We follow the same setup as in [Chen et al., 2023] and replace the OT based training loss with the COT loss described in Section 4.4. In Figure 10, we illustrate our approach to learning the conditional transport plans in the prompt learning setup. We train using SGD with a learning rate $1e-2$ for 50 epochs. Our optimal λ values for different shots (K) are: 10 for $K = 2$, 0.01 for $K = 4$, 0.01 for $K = 8$ and 0.1 for $K = 16$.

7.4 Reproducibility

We have followed standard protocols for ensuring reproducibility in our experiments. We will open-source our code upon acceptance of the paper.

7.5 Future Work

In this paper, we validate the correctness of our estimator for conditional OT and show its utility in downstream applications for a biology task and vision-related tasks. However, we believe that the proposed formulation can be applied to a range of tasks across machine learning domains, which we would like to explore in the near future.

7.6 Negative Societal Impact

We present a formulation for solving optimal transport between conditional distributions. This problem has many socially beneficial applications, like predicting cell responses to cancer treatment, as shown in our paper. However, if a malicious task is selected, the proposed COT formulation may have a negative societal impact, similar to most other methods in machine learning.

8 Funding Disclosure and Acknowledgements

The first author is supported by the Google PhD Fellowship. We thank Fujitsu R&D, Japan International Cooperation Agency and IIT-Hyderabad for the provision of GPU servers used for this work. We thank Pratik Jawanpuria for the insightful discussions, which helped us in formulating our method and in shaping the experimental section. We also thank Amit Chandak for his help during the initial phase of this project.

References

- [Bojanowski et al., 2017] Bojanowski, P., Grave, E., Joulin, A., and Mikolov, T. (2017). Enriching word vectors with subword information. *Transactions of the Association for Computational Linguistics*, 5:135–146.
- [Bunne et al., 2022] Bunne, C., Krause, A., and Cuturi, M. (2022). Supervised training of conditional monge maps. In Koyejo, S., Mohamed, S., Agarwal, A., Belgrave, D., Cho, K., and Oh, A., editors, *Advances in Neural Information Processing Systems*, volume 35, pages 6859–6872. Curran Associates, Inc.
- [Bunne et al., 2021a] Bunne, C., Stark, S. G., Gut, G., del Castillo, J. S., Lehmann, K.-V., Pelkmans, L., Krause, A., and Ratsch, G. (2021a). Learning single-cell perturbation responses using neural optimal transport. *bioRxiv*.
- [Bunne et al., 2021b] Bunne, C., Stark, S. G., Gut, G., del Castillo, J. S., Lehmann, K.-V., Pelkmans, L., Krause, A., and Ratsch, G. (2021b). Learning single-cell perturbation responses using neural optimal transport. *bioRxiv*.
- [Cao et al., 2022] Cao, Z., Xu, Q., Yang, Z., He, Y., Cao, X., and Huang, Q. (2022). Otkge: Multi-modal knowledge graph embeddings via optimal transport. In Koyejo, S., Mohamed, S., Agarwal, A., Belgrave, D., Cho, K., and Oh, A., editors, *Advances in Neural Information Processing Systems*, volume 35, pages 39090–39102. Curran Associates, Inc.
- [Chen et al., 2023] Chen, G., Yao, W., Song, X., Li, X., Rao, Y., and Zhang, K. (2023). Prompt learning with optimal transport for vision-language models. In *ICLR*.
- [FAtlas et al., 2021] Atlas, K., Séjourné, T., Courty, N., and Flamary, R. (2021). Unbalanced minibatch optimal transport; applications to domain adaptation. In *Proceedings of the 38th International Conference on Machine Learning*.
- [FAtlas et al., 2020] Atlas, K., Zine, Y., Flamary, R., Gribonval, R., and Courty, N. (2020). Learning with minibatch wasserstein: asymptotic and gradient properties. In *AISTATS*.
- [Frogner et al., 2015] Frogner, C., Zhang, C., Mobahi, H., Araya, M., and Poggio, T. A. (2015). Learning with a wasserstein loss. In Cortes, C., Lawrence, N., Lee, D., Sugiyama, M., and Garnett, R., editors, *Advances in Neural Information Processing Systems*, volume 28. Curran Associates, Inc.
- [Grünwälder et al., 2012] Grünwälder, S., Lever, G., Gretton, A., Baldassarre, L., Patterson, S., and Pontil, M. (2012). Conditional mean embeddings as regressors. In *Proceedings of the 29th International Conference on Machine Learning, ICML 2012, Edinburgh, Scotland, UK, June 26 - July 1, 2012*. icml.cc / Omnipress.
- [Hahn et al., 2019] Hahn, P. R., Dorie, V., and Murray, J. S. (2019). Atlantic causal inference conference (acic) data analysis challenge 2017.
- [Helber et al., 2019] Helber, P., Bischke, B., Dengel, A., and Borth, D. (2019). Eurosat: A novel dataset and deep learning benchmark for land use and land cover classification.

- [Jawanpuria et al., 2021] Jawanpuria, P., Satyadev, N., and Mishra, B. (2021). Efficient robust optimal transport with application to multi-label classification. In *2021 60th IEEE Conference on Decision and Control (CDC)*, page 1490–1495. IEEE Press.
- [Korotin et al., 2023] Korotin, A., Selikhanovych, D., and Burnaev, E. (2023). Neural optimal transport. In *The Eleventh International Conference on Learning Representations*.
- [Krizhevsky et al., 2009] Krizhevsky, A., Hinton, G., et al. (2009). Learning multiple layers of features from tiny images.
- [Lampert et al., 2009] Lampert, C. H., Nickisch, H., and Harmeling, S. (2009). Learning to detect unseen object classes by between-class attribute transfer. In *2009 IEEE Conference on Computer Vision and Pattern Recognition*, pages 951–958.
- [LeCun and Cortes, 2010] LeCun, Y. and Cortes, C. (2010). MNIST handwritten digit database.
- [Liu et al., 2020] Liu, Y., Zhu, L., Yamada, M., and Yang, Y. (2020). Semantic correspondence as an optimal transport problem. In *Proceedings of the IEEE/CVF Conference on Computer Vision and Pattern Recognition*, pages 4463–4472.
- [Lotfollahi et al., 2021] Lotfollahi, M., Susmelj, A. K., Donno, C. D., Ji, Y., Ibarra, I. L., Wolf, F. A., Yakubova, N., Theis, F. J., and Lopez-Paz, D. (2021). Learning interpretable cellular responses to complex perturbations in high-throughput screens. *bioRxiv*.
- [Makkuva et al., 2020] Makkuva, A., Taghvaei, A., Oh, S., and Lee, J. (2020). Optimal transport mapping via input convex neural networks. In III, H. D. and Singh, A., editors, *Proceedings of the 37th International Conference on Machine Learning*, volume 119 of *Proceedings of Machine Learning Research*, pages 6672–6681. PMLR.
- [Manupriya et al., 2023] Manupriya, P., Nath, J. S., and Jawanpuria, P. (2023). Mmd-regularized unbalanced optimal transport.
- [Maurer, 2016] Maurer, A. (2016). A vector-contraction inequality for rademacher complexities. In Ortner, R., Simon, H. U., and Zilles, S., editors, *Algorithmic Learning Theory*, pages 3–17, Cham. Springer International Publishing.
- [Muandet et al., 2017] Muandet, K., Fukumizu, K., Sriperumbudur, B., and Schölkopf, B. (2017). Kernel mean embedding of distributions: A review and beyond. *Foundations and Trends® in Machine Learning*, 10(1-2):1–141.
- [Peyré and Cuturi, 2019] Peyré, G. and Cuturi, M. (2019). Computational optimal transport. *Foundations and Trends® in Machine Learning*, 11(5-6):355–607.
- [Peyré and Cuturi, 2020] Peyré, G. and Cuturi, M. (2020). Computational optimal transport.
- [Sriperumbudur et al., 2011] Sriperumbudur, B. K., Fukumizu, K., and Lanckriet, G. R. G. (2011). Universality, characteristic kernels and rkhs embedding of measures. *J. Mach. Learn. Res.*, 12(null):2389–2410.
- [Stathias et al., 2018] Stathias, V., Jermakowicz, A. M., Maloof, M. E., Forlin, M., Walters, W. M., Suter, R. K., Durante, M. A., Williams, S. L., Harbour, J. W., Volmar, C.-H., Lyons, N. J., Wahlestedt, C., Graham, R. M., Ivan, M. E., Komotar, R. J., Sarkaria, J. N., Subramanian, A., Golub, T. R., Schürer, S. C., and Ayad, N. G. (2018). Drug and disease signature integration identifies synergistic combinations in glioblastoma. *Nature Communications*, 9.
- [Tabak et al., 2021] Tabak, E. G., Trigila, G., and Zhao, W. (2021). Data driven conditional optimal transport. *Mach. Learn.*, 110(11):3135–3155.
- [Wolf et al., 2018] Wolf, F. A., Angerer, P., and Theis, F. J. (2018). Scanpy: large-scale single-cell gene expression data analysis. *Genome Biology*, 19(1):15.
- [Zhang et al., 2021] Zhang, R., Fang, R., Gao, P., Zhang, W., Li, K., Dai, J., Qiao, Y., and Li, H. (2021). Tip-adapter: Training-free clip-adapter for better vision-language modeling. *arXiv preprint arXiv:2111.03930*.
- [Zhou et al., 2022a] Zhou, K., Yang, J., Loy, C. C., and Liu, Z. (2022a). Conditional prompt learning for vision-language models. In *IEEE/CVF Conference on Computer Vision and Pattern Recognition (CVPR)*.
- [Zhou et al., 2022b] Zhou, K., Yang, J., Loy, C. C., and Liu, Z. (2022b). Learning to prompt for vision-language models. *Int. J. Comput. Vision*, 130(9):2337–2348.